Arbitrarily Shaped Microstrip Structures and Their Analysis with a Mixed Potential Integral Equation

JUAN R. MOSIG, MEMBER, IEEE

Abstract —This paper gives a comprehensive description of the mixed potential integral equation (MPIE) as applied to microstrip structures. This technique uses Green's functions associated with the scalar and vector potential which are calculated by using stratified media theory and are expressed as Sommerfeld integrals. Several methods of moments allowing the study of irregular shapes are described. It is shown that the MPIE includes previously published static and quasi-static integral equations. Hence, it can be used at any frequency ranging from dc to higher order resonances. Several practical examples including an L-shaped patch have been numerically analyzed and the results are found to be in good agreement with measurements.

I. INTRODUCTION

THE PRACTICAL advantages of microstrip structures have been discussed in many papers and are now too well known to be repeated here. On the other hand, it is perhaps worthwhile to point out that such structures are very well suited for mathematical modeling. This seldom mentioned "theoretical" advantage is mostly due to the relatively simple geometry of microstrip structures and has certainly contributed to their popularity. Indeed, every analytical technique commonly used in electromagnetics has been applied to microstrip, giving rise to a surprisingly great number of different and apparently unrelated models.

In this paper, we will put the emphasis on the analysis of microstrip structures having upper conductors of arbitrary shape. The general term *microstrip structures* includes here patches of finite size and discontinuities obtained by interconnecting several microstrip lines through a patch.

The purpose of many microstrip models is to provide an equivalent circuit for a given structure. The simplest models yield lumped *LC* circuits, valid at low frequencies. Improvements of these models introduce ohmic losses (a series resistance) and dielectric losses (a parallel conductance). At higher frequencies, the microstrip structure can no longer be represented by a classical *RLC* circuit. More accurate models are then employed that take into account the dynamic behavior of the fields and yield scattering or impedance matrices with, in general, complex elements varying with frequency. If the field analysis is made for an open microstrip structure, the port matrices (S or Z) should include real terms accounting for the radiation losses (surface and space waves).

Equivalent capacitances and inductances of a microstrip structure can be obtained by solving, respectively, a static integral equation [1], [2] and a quasi-static integral equation [3], [4]. But these models are restricted to low frequencies, where the real part of any impedance parameter is negligible and the imaginary part behaves like the reactance of a classical *LC* circuit.

A more accurate model including dispersion is the waveguide/cavity model which leads directly to the scattering matrix of the structure [5]. However, this model neglects fringing fields as well as radiation and surface waves. Therefore it is restricted to electrically thin substrates. The same restriction applies to models based upon the planar circuit concept [6]–[8].

The most general and rigorous treatment of microstrip structures is given by the well-known electric field integral equation (EFIE) technique, usually formulated in the spectral domain [10], [11]. In this paper, we use a modification of the EFIE, called the mixed potential integral equation (MPIE), and we solve it in the space domain. The MPIE is numerically stable and can be solved with efficient algorithms [12]. Working in the space domain helps to keep a good physical insight of the problem.

The MPIE was introduced by Harrington [13] and has been extensively used for the analysis of wire antennas. Here, the MPIE will be applied to microstrip introducing specific kernels which account for dielectric layers and for the ground plane. It is shown that the MPIE models can be used at any frequency, from the static case up to the determination of higher order modes in a resonant patch. Several specializations to particular frequency ranges are discussed in detail. Also, this formulation includes coupling, dispersion, radiation losses, and surface waves and therefore provides a powerful and flexible technique for the study of microstrip structures.

II. THE MPIE FOR MICROSTRIP STRUCTURES

A. Initial Assumptions

We consider here microstrip structures where the substrate and the ground plane have infinite transverse dimensions (Fig. 1a). Theoretical developments are given here for
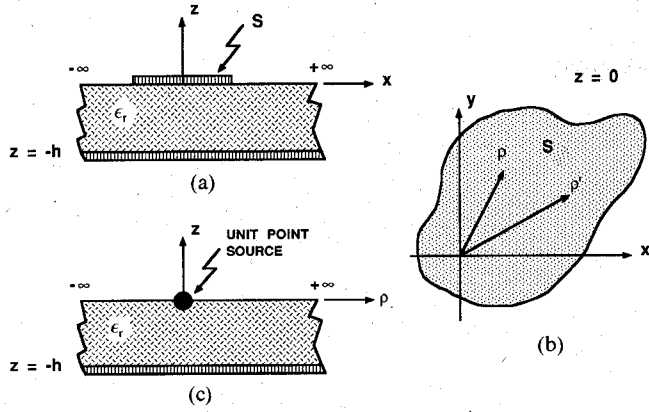
Fig. 1. (a) $y-z$ plane cut and (b) $x-y$ plane cut of a microstrip structure and (c) associated problem for the evaluation of the Green functions.

a single-layer substrate. Modifications needed to account for multiple layers will be mentioned later on. Ohmic losses in the upper conductor are included by introducing a surface impedance equal to the ratio of the tangential electric field to the surface current density. If standard thin-film technology is used, the upper conductor thickness (25–50 μm) can be neglected against substrate thickness, but is still many times greater than the skin depth at microwave frequencies (6 μm for copper at 1 GHz). Hence the upper conductor is modeled as an electric current sheet and the surface impedance can be estimated as

$$Z_s = (1 + j)\sqrt{\pi f \mu_0/\sigma}. \tag{1}$$

Dielectric losses will be accounted for by introducing, as customary, a complex dielectric constant:

$$\epsilon_r = \epsilon_r'(1 - j\tan\delta). \tag{2}$$

Ohmic losses in the ground plane can be taken into account by modifying the Green's functions of the problem [14]. A simplified procedure keeps the Green's functions associated with an ideal ground plane and doubles the resistivity of the upper conductor.

As mentioned in the introduction, radiation and surface waves are automatically included in this formulation. Finally, the convention $\exp(j\omega t)$ will be used throughout the paper.

B. The Integral Equation

To set up an integral equation for the currents and the charges, we start with the boundary condition associated with the tangential electric field in the surface S of the upper conductor (Fig. 1(b)):

$$e_z \times [E^{(e)} + E^{(s)}] = Z_s J_s. \tag{3}$$

Here, $E^{(e)}$ is the excitation field and $E^{(s)}$ is the scattered field, which can be derived from a scalar potential V and a vector potential A as

$$E^{(s)} = -j\omega A - \nabla V. \tag{4}$$

These potentials are in turn expressed, by means of the corresponding Green's functions $G_V, \overline{\overline{G}}_A$, as superposition

integrals of the charge and current densities q_s and J_s:

$$V(\rho) = \int_S ds' G_V(\rho|\rho') q_s(\rho') \tag{5}$$

$$A(\rho) = \int_S ds' \overline{\overline{G}}_A(\rho|\rho') \cdot J_s(\rho'). \tag{6}$$

Finally, the MPIE can be written as

$$e_z \times E^{(e)}(\rho) = e_z \times \left[j\omega \int_S ds' \overline{\overline{G}}_A(\rho|\rho') \cdot J_s(\rho') \right.$$
$$\left. + \nabla \int_S ds' G_V(\rho|\rho') q_s(\rho') + Z_s J_s(\rho) \right] \tag{7}$$

where charge and current densities are related through the continuity equation

$$\nabla \cdot J_s + j\omega q_s = 0.$$

Rigorously, the MPIE is a Fredholm integral of the second kind, but the term $Z_s J_s$ is usually small and the MPIE behaves numerically as a Fredholm integral to the first kind. Prior to solving (7) numerically with a method of moments, the Green's functions must be evaluated. These functions correspond physically to the potentials created by unit point sources (Fig. 1(c)). Hence, their determination can be done in the $\rho-z$ plane. Once the Green's functions are computed and stored for the case $z = 0$, we can get rid of the z coordinate and perform all the subsequent calculations in the $x-y$ plane of Fig. 1(b). In general, integral equation techniques reduce one 3-D problem $(x-y-z)$ to two 2-D problems $(\rho-z$ and $x-y)$ resulting in a numerically efficient approach. For instance, going from free-space to multilayered substrates requires only a modification of the Green's functions, but the 2-D problem in the $x-y$ plane remains unchanged.

C. The Green's Functions

A thorough study of the Green's functions for microstrip structures can be found in previous works by the author [15]. For sake of completeness, we will mention here the final results for a single layer and for $z = 0$.

For the dyadic $\overline{\overline{G}}_A$, we consider only its x, y components, since neither the z component of the current nor the z component of the electric field need to be considered in (7). By symmetry considerations, we have

$$G_V(\rho|\rho') = G_V(\rho - \rho'|0) = g_V(|\rho - \rho'|) \tag{8}$$

$$G_A^{st}(\rho|\rho') = G_A^{st}(\rho - \rho'|0) = \begin{cases} g_A(|\rho - \rho'|) & st = xx, yy \\ 0 & st = xy, yx. \end{cases} \tag{9}$$

The Green's functions g_V and g_A show translational invariance in the $x-y$ plane and therefore are only functions of the source–observer distance $R = |\rho - \rho'|$. Their expressions in terms of Sommerfeld integrals are [15]:

$$2\pi\epsilon_0 g_V(R) = \int_0^\infty d\lambda \, J_0(\lambda R)\frac{\lambda(u_0 + u\tanh uh)}{D_{TE} D_{TM}} \tag{10}$$

$$(2\pi/\mu_0)g_A(R) = \int_0^\infty d\lambda \, J_0(\lambda R)\frac{\lambda}{D_{TE}} \tag{11}$$

where

$$D_{TE} = u_0 + u \coth uh \qquad D_{TM} = \epsilon_r u_0 + u \tanh uh$$

and

$$u_0 = \sqrt{\lambda^2 - k_0^2} \qquad u = \sqrt{\lambda^2 - \epsilon_r k_0^2}$$

with λ being the dummy spectral variable.

TE (TM) surface waves appear as zeros of D_{TE} (D_{TM}) and hence as poles of the functions to be integrated in (10) and (11). It is worth pointing out that the result (9) stems from the fact that the traditional approach of Sommerfeld is used. However, it has been recently shown [16] that this approach should be modified if the conductors are not restricted to horizontal planes, in order to keep the unicity of the scalar Green's function G_V.

Stratified-media theory [17] allows the generalization of (9) and (10) to multilayered substrates. The two-layer case has been recently investigated in connection with microstrip radome problems [18].

Efficient numerical evaluation of the integrals (10) and (11) calls for quite sophisticated techniques [15]. Nevertheless, since the integrals are functions of only one space variable, namely the source–observer distance, they can be precomputed for a given range of values and stored as

D. Space and Spectral Domains

The MPIE deserves the qualification of the space-domain technique because once the Green's functions have been computed, we get rid of the spectral variable λ and the integral equation is effectively solved in the $x - y$ plane. On the contrary, the spectral domain EFIE [10], [11] keeps the calculations in the spectral plane until the final steps. But it must be emphasized that both models are physically equivalent and their differences are purely numerical. Indeed, they are both rigorously derived from Maxwell's equations and if no approximations are made in their numerical treatment, they should provide identical results.
results.

III. Specializations of the MPIE

Fig. 2(a) shows a microstrip structure with two ports. The excitation fields are produced by an ac generator connected to the input port, while the output port is loaded by an arbitrary impedance. Surface currents and charges exist in the upper conductor and from them the port impedance matrix can be determined.

From a circuit point of view, two particular cases deserve consideration. In the first one (Fig. 2(c)) the generator is a dc battery and the load is an open circuit. No current flow exists, and the sole unknown is the charge density, whose determination allows the computation of the capacitance of the microstrip structure. In the second case, we have a low-frequency current generator at the input port and a short circuit at the output port (Fig. 2(b)). A divergenceless surface current flows through the closed circuit. There is no surface charge and $I_1 = -I_2$. From the surface current, an inductance associated with the microstrip structure can be determined.
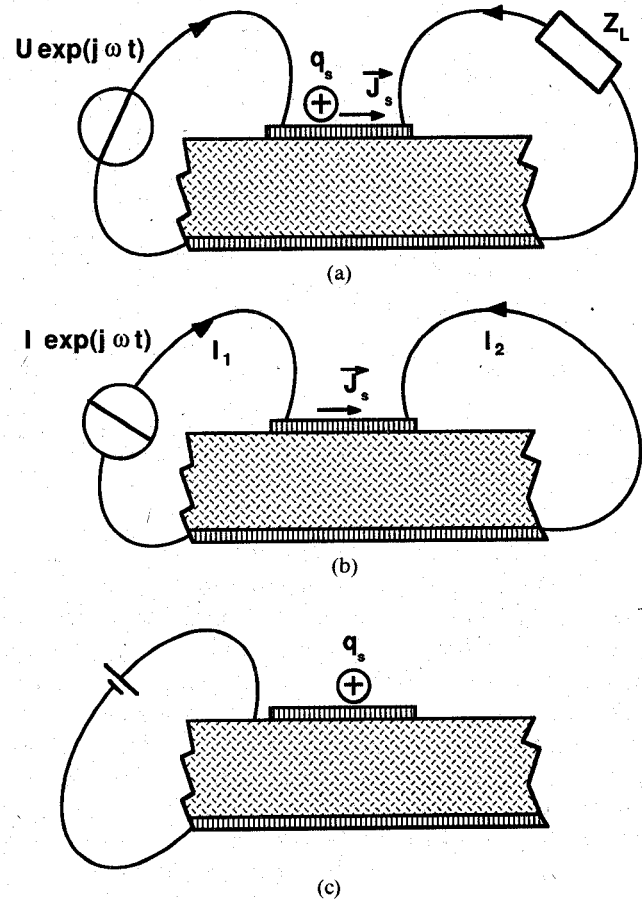

Fig. 2. Three possible excitations of a microstrip circuit: (a) dynamic (time-harmonic), (b) quasi-static and (c) static.

Both cases are included in the MPIE model and give rise, respectively, to static and quasi-static specializations of the MPIE.

A. The Static Case

In the absence of currents, (7) becomes

$$e_z \times \nabla \int_S ds' G_V(\rho|\rho') q_s(\rho') = e_z \times E^{(e)}(\rho). \qquad (12)$$

In many practical situations, it is customary to assume that the excitation field is created by some charge distribution $q_s^{(e)}$ via the same Green's function. Then, (12) can be rewritten as

$$e_z \times \nabla \int_S ds' G_V(\rho|\rho') [q_s^{(e)}(\rho') + q_s(\rho')] = 0 \qquad (13)$$

which implies, by integration over the tangential coordinates, that

$$\int_S ds' G_V(\rho|\rho') [q_s^{(e)}(\rho') + q_s(\rho')] = \text{constant} = U. \qquad (14)$$

Instead of starting with an excitation charge, solving (13) for the "scattered charge" q_s, and finally computing the voltage U with (14), it will frequently be easier to start by assuming the voltage U known and considering (14) as an integral equation for the total charge $q_s^{(e)} + q_s$. This last approach follows closely the circuit representation of Fig. 2(c), and corresponds to the well-known static integral

equation for the evaluation of capacitances. The Green's function to be used in (12)–(14) can be found by setting $k_0 = 0$ in the general expression (10). The result is

$$2\pi\epsilon_0 g_V(R) = \int_0^\infty d\lambda\, J_0(\lambda R)(1 + \epsilon_r \coth \lambda h)^{-1} \quad (15)$$

or, expanding the sum inside the parentheses into powers of $\exp(-2\lambda h)$ and integrating the resulting infinite series term by term,

$$4\pi\epsilon_0 g_V(R) = (1-\eta)\left[\frac{1}{R_0} - (1+\eta)\sum_{n=1}^\infty (-\eta)^{n-1}\frac{1}{R_n}\right] \quad (16)$$

with

$$\eta = (\epsilon_r - 1)/(\epsilon_r + 1) \qquad R_n^2 = R^2 + 4n^2 h^2.$$

The series (16) is the well-known partial image representation of the static Green's function, given by Silvester [19], while the integral representation (15) was first used by Patel [20]. Generalizations of (15) to multilayered substrates can be found in [21].

B. The Quasi-Static Case

The classical technique to obtain an approximated integral equation useful at low frequencies implies neglecting losses and displacement currents. Taking the divergence of (7) with $Z_s = 0$ gives

$$j\omega e_z \cdot \nabla \times \int_S ds'\,\overline{\overline{G}}_A(\rho|\rho') \cdot J_s(\rho') = e_z \cdot \nabla \times E^{(e)}(\rho)$$

$$= -j\omega\mu_0 e_z \cdot H^{(e)}(\rho) \quad (17)$$

where the equivalence $\nabla \cdot (e_z \times X) = e_z \cdot (\nabla \times X)$ has been used. Introducing now the del operator under the integration sign leads to

$$e_z \cdot \int_S ds'\,\overline{\overline{G}}_H(\rho|\rho') \cdot J_s(\rho') + e_z \cdot H^{(e)}(\rho) = 0 \quad (18)$$

where the dyadic Green function associated with the magnetic field is $\mu_0 \overline{\overline{G}}_H = \nabla \times \overline{\overline{G}}_A$. According to (9), its relevant components are given by

$$\mu_0 G_H^{zx} = -\partial g_A/\partial y \qquad \mu_0 G_H^{zy} = \partial g_A/\partial x. \quad (19)$$

Equation (18) simply expresses the fact that the total normal magnetic field must vanish on the surface of lossless conductors at any frequency. However, since (18) is a scalar equation, it does not suffice in general to determine the two components of the surface current. The second scalar equation is obtained by neglecting the displacement current in Maxwell's equations. Then $\nabla \times H = J$ and, consequently, J_s is solenoidal, i.e.,

$$\nabla \cdot J_s = 0. \quad (20)$$

The set of equations (18)–(20) defines the quasi-static model.

As in the static case, it will sometimes be convenient to introduce an excitation current $J_s^{(e)}$. Then, (18) is transformed into

$$e \cdot \int_S ds'\,\overline{\overline{G}}_H(\rho|\rho') \cdot \left[J_s(\rho') + J_s^{(e)}(\rho')\right] = 0 \quad (21)$$

and the system of equations (20) and (21) is solved taking into account the additional condition

$$\int_C dl\, e_n \cdot J_s = I \quad (22)$$

which relates the excitation surface current to the total current entering the structure in Fig. 2(b).

Since displacement currents are neglected, the current distribution satisfies a static Poisson equation. Consequently, to ensure the internal coherence of the model, the Green's functions arising in (17), (18), and (21) must be static too. At zero frequency, (11) becomes

$$(4\pi/\mu_0)g_A(R) = 2\int_0^\infty d\lambda\, J_0(\lambda R)(1 + \coth \lambda h)^{-1}$$

$$= \left(\frac{1}{R} - \frac{1}{\sqrt{R^2 + 4h^2}}\right) \quad (23)$$

which is the solution to the problem of a point source above a ground plane. Therefore, the quasi-static model is independent on the substrate permitivity.

IV. THE METHOD OF MOMENTS

In order to apply the MPIE to irregular microstrip shapes, we need a very flexible numerical technique. The most frequent choice is a method of moments with subsectional basis functions [13]. In this approach, the upper conductor is divided into elementary domains (cells) and the basis functions defined over each cell. We have chosen the rectangular cell as the simplest shape still able to provide good approximations for many practical structures. More sophisticated shapes for the cells, such as triangles [22] and quadrangles, have been used in scattering problems and could also be applied to microstrip problems.

We also need to select the basis functions. In general, each component of the surface current will depend on the two coordinates x, y, but it is possible to use basis functions which are, inside each cell, constant along the transverse coordinate. This yields expansions for J_{sx} and J_{sy} which are discontinuous along, respectively, y and x, but the associated charge is still nonsingular. Basis functions ensuring continuity of the current in any direction, such as bilinear expansions, may be used, but the improved accuracy of the results is balanced by the increased difficulty of the computations.

The choice of test functions is also a crucial matter. To illustrate this, three possible combinations of basis and test functions will be described (Fig. 3). Other possibilities are given in [25].

Case A) Rooftop and Galerkin

An interesting possibility is using overlapping rooftop functions for the two components of the surface current (Fig. 3(a)). Then, according to the continuity equation, the basis functions for q_s are 2-D pulse doublets. The MPIE is tested by using the same rooftop functions and this yields a Galerkin procedure.

Define T_t as the vector rooftop function associated with two adjacent cells S_i^+ and S_i^- (Fig. 4(a)). The union of

Fig. 3. Some possible choices for the basis and test functions defined over rectangular domains. All the two-dimensional functions considered are independent of the transverse coordinate.
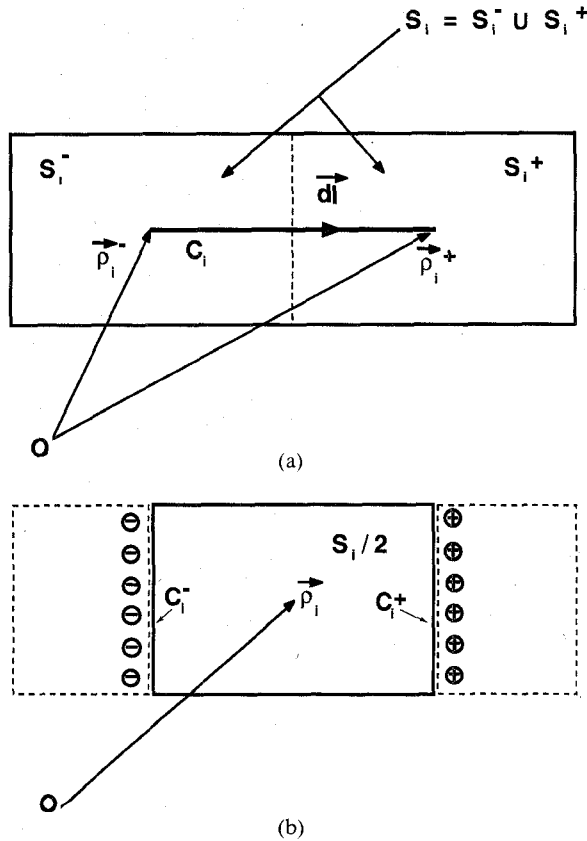

(a)

(b)

Fig. 4. (a) Longitudinal testing segments C_i linking the centers of adjacents cells (S_i^- and S_i^+) and (b) transverse segments (C_i^- and C_i^+) containing the line charge densities in the point-matching approach.

these two cells will be simply denoted by S_i. In general, we need to consider N_x x-directed functions and N_y y-directed functions, the total number being $N = N_x + N_y$. Therefore,

$$T_i = \begin{cases} e_x T_{ix} & i = 1, 2 \cdots N_x \\ e_y T_{iy} & i = N_x + 1 \cdots N. \end{cases} \qquad (24)$$

The current and the charge are expanded as

$$J_s = \sum_{i=1}^{N} \alpha_i T_i \qquad j\omega q_s = \sum_{i=1}^{N} \alpha_i \Pi_i \qquad (25)$$

where the α_i are unknown coefficients and the functions $\Pi_i = -\nabla \cdot T_i$ correspond to the pulse doublets.

Standard application of the method of moments yields a matrix equation with the elements of the matrix given by

$$z_{ij} = a_{ij} + v_{ij} + l_{ij} \qquad (26)$$

where the contribution of $\overline{A}, V$, and the ohmic losses are, respectively,

$$a_{ij} = j\omega \int_{S_i} ds \, T_i(\rho) \cdot \int_{S_j} ds' \overline{\overline{G}}_A(\rho|\rho') \cdot T_j(\rho') \qquad (27)$$

$$v_{ij} = \frac{1}{j\omega} \int_{S_i} ds \, \Pi_i(\rho) \int_{S_j} ds' G_V(\rho|\rho') \Pi_j(\rho') \qquad (28)$$

$$l_{ij} = Z_s \int_{S_i} ds \, T_i(\rho) \cdot T_j(\rho). \qquad (29)$$

Notice that a_{ij} vanishes if T_i is perpendicular to T_j, while $l_{ij} = 0$ if there is no intersection between S_i and S_j. In general the computation of each matrix element requires a fourfold integral. Even if two integrals can be evaluated analytically through an adequate change of variables, this approach remains cumbersome and simpler possibilities must be investigated.

Case B) Rooftop and Testing Along Segments

This modification has been suggested by Glisson and Wilton [12] and successfully applied to microstrip resonators and antennas [23].

The basis functions are the same as in A) but testing is done along the segment C_i linking the centers of cells S_i^+ and S_i^- (Fig. 4(a)). Thus we get, instead of (27)–(29),

$$a_{ij} = j\omega \int_{C_i} dl \cdot \int_{S_j} ds' \overline{\overline{G}}_A(\rho|\rho') \cdot T_j(\rho') \qquad (30)$$

$$v_{ij} = \frac{1}{j\omega} \int_{S_j} ds' \left[G_V(\rho_i^+|\rho') - G_V(\rho_i^-|\rho') \right] \Pi_j(\rho') \qquad (31)$$

$$l_{ij} = Z_s \int_{C_i} dl \cdot T_j(\rho) \qquad (32)$$

where ρ_i^+, ρ_i^- denote the centers of the cells S_i^+, S_i^-. These expressions, simpler than (27)–(29), can be brought to effective numerical evaluation [23].

In Section III, we have mentioned the fact that the MPIE remains valid at low frequency and tends to the static integral equation. However, the condition of the matrix of moments worsens when the frequency decreases, thus preventing accurate results. This drawback can be removed by testing along the segments belonging to an open tree and replacing the remaining segments by closed loops [24]. According to Faraday's law, a null circulation of the electric field along closed loops is equivalent to enforcing a zero average value of the normal magnetic field inside the loop. Hence, the quasi-static integral equation (21) is included in the MPIE.

Case C) 2-D Pulses and Point Matching

The simplest, but still meaningful, combination of basis and test functions expands the components of the current over a set of 2-D pulses. In order to approximately satisfy the appropriate edge conditions on the surface current, these pulses are defined over domains which do not coincide with the original cells. Rather, each domain, symbolically denoted by $S_i/2$, is a combination of two cell's halves and can be considered as a two-dimensional extension of the segment C_i (Fig. 4(b)).

The associated charges are now line charges (Dirac's delta functions) distributed along two segments C_i^+ and C_i^- (Fig. 4(b)). Testing the MPIE is performed by point matching at the centers of segments C_i. Only the component of the electric field parallel to the segment is tested. A general matrix element is still given by (26), but now we have

$$a_{ij} = j\omega e_i \cdot \int_{S_j/2} ds' \overline{\overline{G}}_A(\rho_i|\rho') \cdot e_j \tag{33}$$

$$v_{ij} = \frac{1}{j\omega} \int_{C_i^+} dl' G_V(\rho_i|\rho') - \frac{1}{j\omega} \int_{C_i^-} dl' G_V(\rho_i|\rho') \tag{34}$$

$$l_{ij} = \hat{Z}_s \delta_{ij} \tag{35}$$

where δ_{ij} is the Kronecker symbol and $e_i(e_j)$ is a unit vector parallel to $C_i(C_j)$.

The Numerical Integration Problem

The differences between the several combinations of basis and test functions disappear if an inaccurate numerical integration is used. For instance, it is meaningless to apply a Galerkin approach of type A) and then perform the integrations in (27)–(29) by using the mean-value theorem, because the resulting algorithm will be more like a point-matching technique. In this sense, the technique B) can be considered a particular version of A) using a rather loose integration technique.

A simplification of technique B) uses for the current 2-D pulses instead of rooftop functions, while keeping the 2-D pulse doublets for the charge [12], [13]. The continuity equation is no longer satisfied, but the approach can be justified on numerical grounds as being technique B) with an approximate surface integration.

V. MATHEMATICAL TREATMENT OF THE EXCITATION

The excitation fields are seldom known in a direct way, except in a few cases, such as exciting with a plane wave or with a series voltage gap generator (very unpractical in microstrip). Therefore, the excitation fields must usually be computed from a given distribution of currents and charges. The simplest model for the excitation is a vertical filament of unit current (Dirac's delta) acting on some point of the upper conductor. This model is a first-order approximation of real-world coaxial pins but can only be used with the method of moments of the type A), where the testing integrations suffice to smooth out the delta's singularity. For techniques B) and C), a more accurate model of the coaxial probe has been developed in [23].
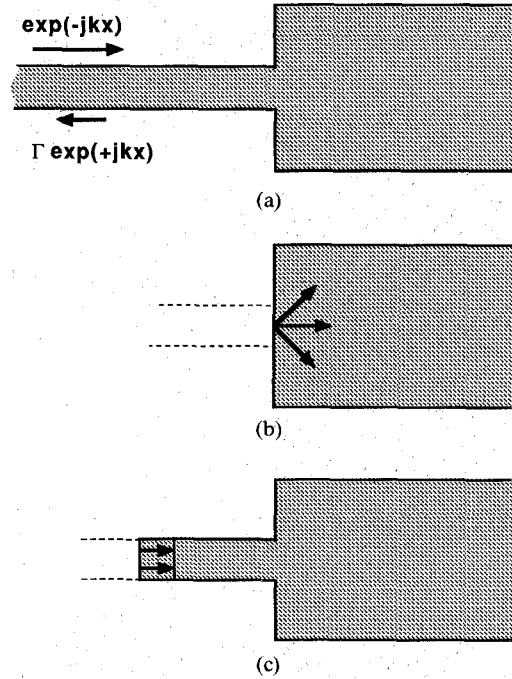

Fig. 5. (a) Microstrip discontinuity showing the incident and reflected waves in the feed line. (b) Approximate model totally neglecting the feed line. (c) Approximate model partially neglecting the feed line. In both (b) and (c) the field analysis yields Z_{in}, and the reflection coefficient is estimated as $(Z_{in} - Z_c)/(Z_{in} + Z_c)$, Z_c being the characteristic impedance of the feed line.

Concerning microstrip-fed structures (Fig. 5(a)), there are several possibilities. The most obvious one neglects the microstrip line in the field analysis and uses a vertical filament at the insertion point in the edge of the patch (Fig. 5(b)). Hence, the mathematical excitation is $J_s = e_z \delta(z)$. A better possibility, including discontinuity effects in the insertion zone, is to include a finite section of the microstrip line in the field analysis and to introduce a series current generator at the point where the line has been truncated (Fig. 5(c)). The generator can be mathematically described by a half-rooftop function bearing a unit current.

These models for the excitation lead to values of the input impedance. A more rigorous approach yielding directly the value of the reflection coefficient would require special basis functions to represent the incident and reflected quasi-TEM waves on the semi-infinite feed line [11].

VI. NUMERICAL RESULTS

A. The Linear Resonator

In order to study the convergence of the results with the number of longitudinal cells, we consider first an open-circuited microstrip line resonator with aspect ratio $L/w = 37.4$ and $\epsilon_r = 1$ (Fig. 6). Since this is a very narrow patch, only longitudinal currents are considered. The numerical algorithms of Section IV, labeled as before A), B), and C), are applied with one cell along the transverse direction and N cells along the longitudinal coordinate. For a fixed N, the modulus of the determinant of the moments' matrix shows a sharp minimum at the resonance. Fig. 6 gives the
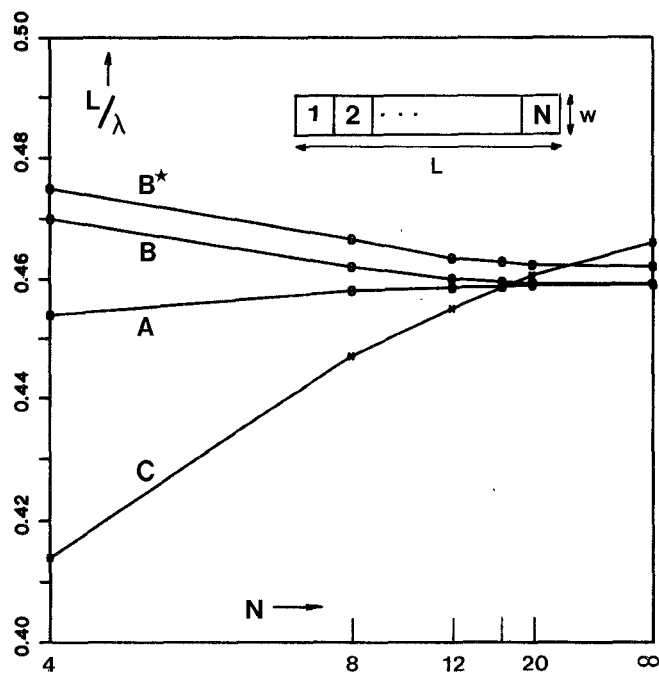
Fig. 6. The narrow linear resonator: convergence of the resonant frequency as a function of the number N of cells for the three techniques of Section IV.

normalized resonant frequency as a function of $1/N$. This allows graphical extrapolation for the case $N = \infty$.

Techniques B) and A) both converge quickly to an extrapolated frequency $L/\lambda_0 = 0.459$, which can be considered "numerically exact." The relative error for $N = 8$ is 0.9 percent for the testing-along segments algorithm B) and only 0.1 percent for the Galerkin algorithm A). On the other hand, point matching C) converges rather slowly and the extrapolated value for infinity is slightly different ($L/\lambda_0 = 0.466$). From the point of view of computation time, B) is three times slower and A) seven times slower than C). Hence the algorithm B) represents a good compromise and cells of length 0.05λ ensure accuracy of 1 percent.

Fig 6 also gives results on a modification of algorithm B) which allows for a transverse variation of the longitudinal current. This modification, denoted B*), accounts for edge effects, with a dependence of the type $[1-(2y/w)^2]^{1/2}$. The predicted resonant frequency changes only by 0.7 percent, and this difference becomes even smaller if more than one cell is allowed in the transverse direction.

B. The Rectangular Patch

The second test case is a wide rectangular patch of length $L = 150$ mm and aspect ratio $L/w = 2$ (Fig. 7). The substrate parameters are $h = 3.175$ mm, $\epsilon_r = 2.56$, and $\tan \delta = 0.0015$.

The patch is excited by a coaxial probe at $x = 58.33$ mm, $y = 37.5$ mm. To study the relevance of the number of transverse cells, numerical tests were made with a number of cells fixed along x ($N = 9$) and variable along y ($M = 3,5,7$). Results for the input impedance near the resonance are presented in the Smith chart of Fig. 7. The
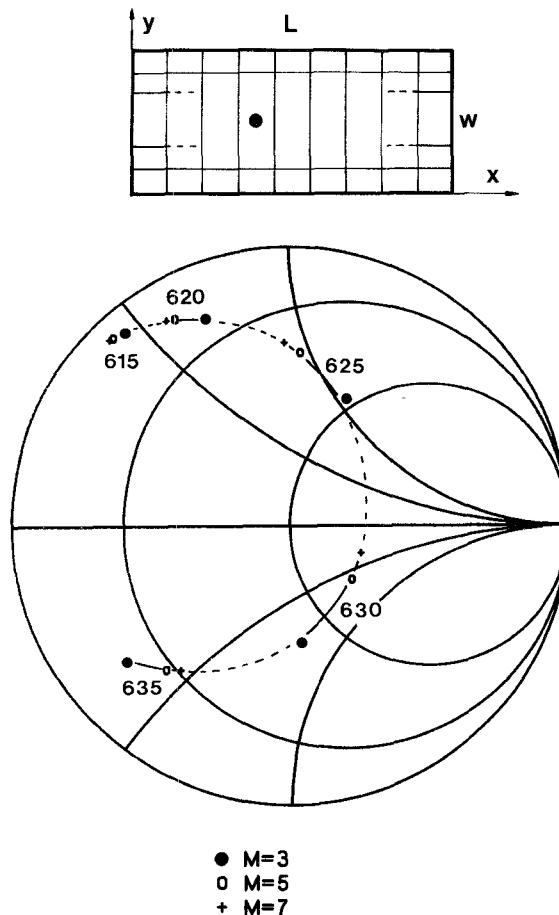

● M=3
0 M=5
+ M=7

Fig. 7. The rectangular patch: convergence of the input impedance as a function of the number of cells in the transverse direction (615–635 MHz).

extrapolated ($M = \infty$) value of the resonant frequency is 628.9 MHz. The error is 0.2 percent for $M = 7$ and still only 0.7 percent for $M = 3$. This shows that the boundary condition imposing infinite values for the current density at the lateral edges can be neglected in the numerical treatment of wide patches, without appreciable loss of accuracy. It is also worth mentioning that all the points in Fig. 7 are almost on the same curve. This means that the impedance level is almost independent of the number of transverse cells, $M > 3$ being enough for engineering accuracy.

The rectangular patch was also analyzed well below the resonance for frequencies ranging from 50 to 500 MHz. The input impedance $R + jX$ normalized to 50 Ω is plotted in Fig. 8. In addition to a small real part, which accounts for ohmic losses, dielectric losses, and radiation, there is a reactance whose limiting value at low frequency is $-1/\omega C_0$ (dashed line), C_0 being the static capacitance of the patch [12].

C. The L-Shaped Patch

To illustrate the performance of the MPIE when dealing with irregular shapes, we have selected an L-shaped patch (Fig. 9(a)). Its dimensions are $a = b = 56$ mm, and $c = d = 28$ mm. The substrate parameters are $\epsilon_r = 4.34$, $\tan \delta = 0.02$,
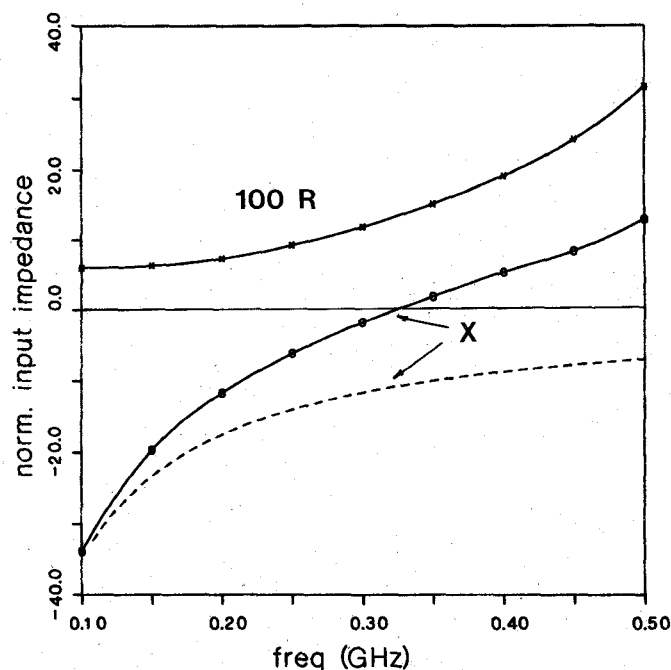
Fig. 8. Normalized input impedance $Z = (R + jX)/50$ Ω of a rectangular patch. The static approximation $Z \cong 1/j\omega C_0$ is given by the dashed line.
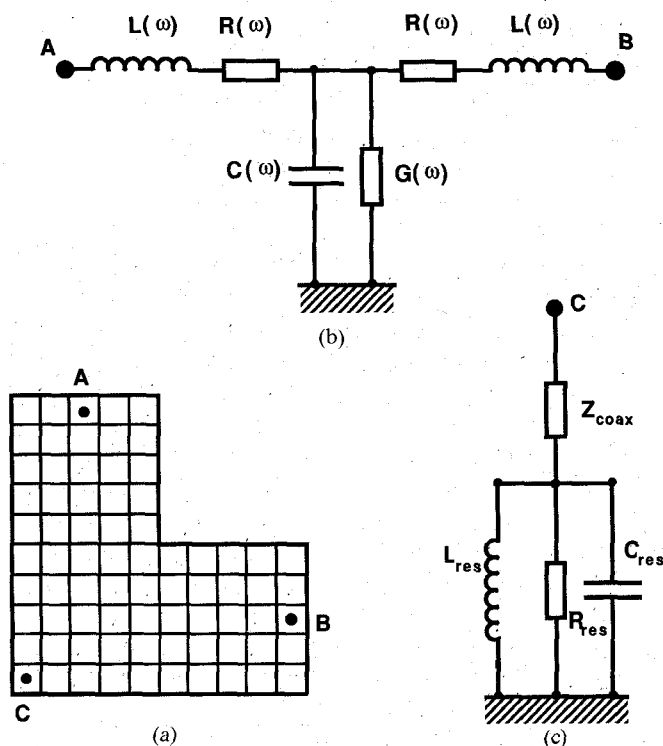

(b)

(a)

(c)

Fig. 9. The L-shaped microstrip patch. (a) Decomposition into elementary cells showing the coaxial-fed ports A, B, C. (b) Equivalent circuit at low frequency for a two-port excitation (A and B). (c) Equivalent circuit near resonance for an one-port excitation (C).

Phase

Max. Value = 0.102 x10** 0 Amps

Quadrature
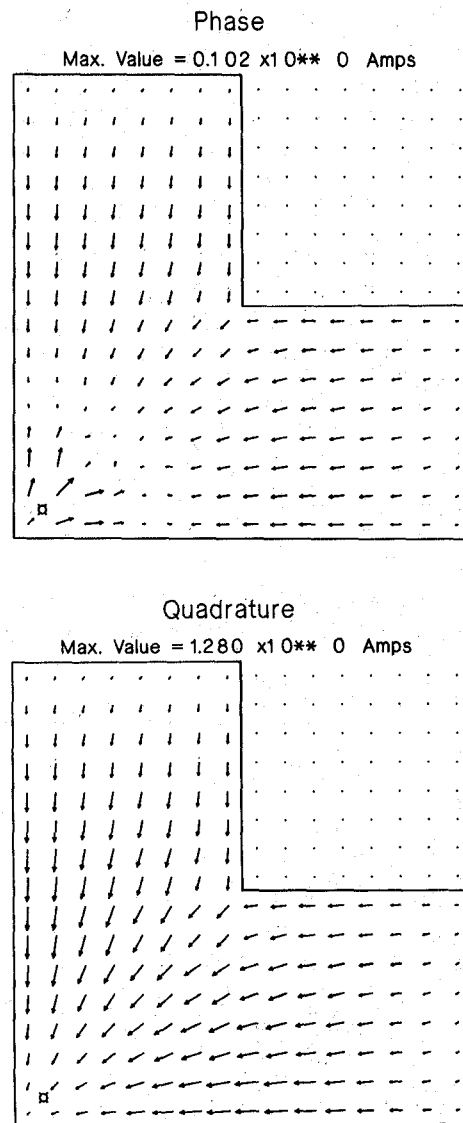
Max. Value = 1.280 x10** 0 Amps

Fig. 10. Real (in-phase) and imaginary (in quadrature) parts of the surface current existing in the L-patch at the second resonance. The maximum value of the current corresponds to the longest arrow. Excitation current in the coaxial is $1 + j0$ A.

and $h = 0.8$ mm, and the patch is divided into 75 square cells.

We looked first for higher order resonances, exciting the patch with a coaxial probe C located at $x = 2.8$ mm, $y = 2.8$ mm. Two resonances were found, at 1.555 GHz and 2.536 GHz. A first resonance, at 0.998 GHz, is missed

due to the symmetrical location of the coaxial probe. Fig. 10 gives a vector representation for the real and imaginary parts of the surface current density when the total excitation current entering the patch is normalized to $1 + j0$ A. As in any resonating situation, the imaginary part is stronger and its pattern is independent of the coaxial position. On the other hand, the real part, neglected in many microstrip models, corresponds to near-field effects created by the coaxial probe. This real part can modify greatly the input reactance values, mainly in weak resonances.

The input impedance at the second resonance is given in Fig. 11 and compared with measurements. The theoretical predictions are very good, with an error of only 1 percent in the resonant frequency, 4 percent in the maximum resistance, and a slight difference in the reactance values. The patch behaves as a parallel resonant circuit with a small series reactance due to the probe (Fig. 9(c)). The
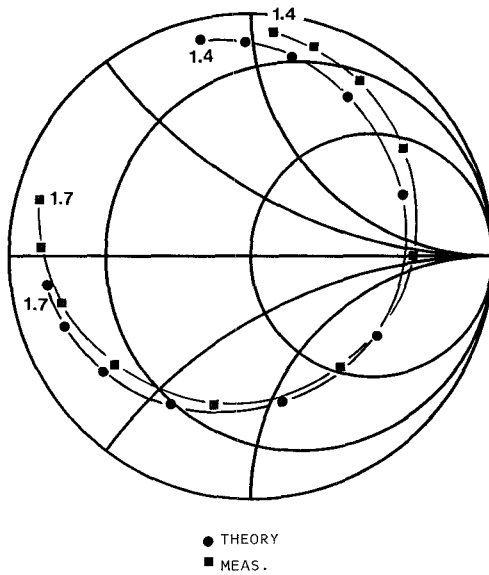
Fig. 11. Input impedance of the L-shaped patch near the second resonance (1.4–1.7 GHz): ● = theory, ■ = measurements.
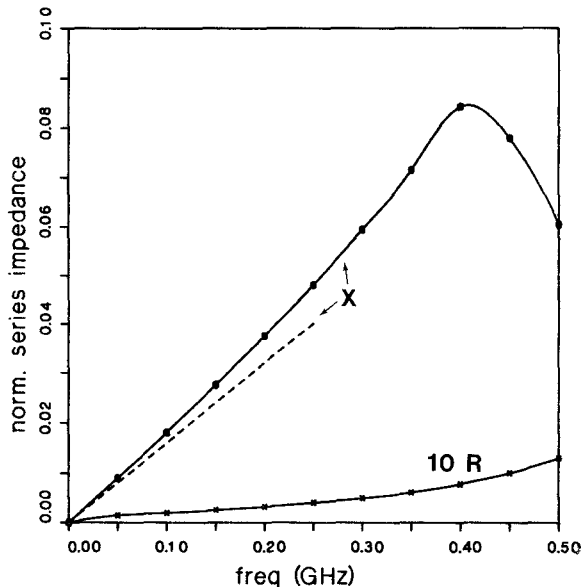

Fig. 12. Normalized series impedance $Z_s = (R + jX)/50$ Ω of an L-shaped patch below the first resonance (see the equivalent circuit of Fig. 9(b)). The dashed line represents the quasi-static approximation $Z_s \cong j\omega L_0/50$ Ω.

Fig. 13. Normalized parallel admittance $Y_p = (G + jB) \times 50$ Ω of an L-shaped patch below the first resonance (see the equivalent circuit of Fig. 9(b)). The dashed line represents the static approximation $Y_p \cong j\omega C_0 \times 50$ Ω.

elements of the equivalent circuit are easily obtained from the input impedance values of Fig. 12.

We have also considered the L-shaped patch as a two-port network with coaxial excitations at points A ($x_A = 8.4$ mm, $y_A = 47.6$ mm) and B ($x_B = 47.6$ mm, $y_B = 8.4$ mm). At low frequency, the patch behaves as a microstrip bend discontinuity and we can assume the equivalent circuit of Fig. 9(b). The normalized values of the series impedance $R(\omega) + jX(\omega)$ and of the parallel admittance $G(\omega) + jB(\omega)$ are given in Figs. 12 and 13. Again, the MPIE predicts correctly the frequency behavior of the structure. In particular, as the frequency goes to zero the reactance and susceptance values tend toward, respec-
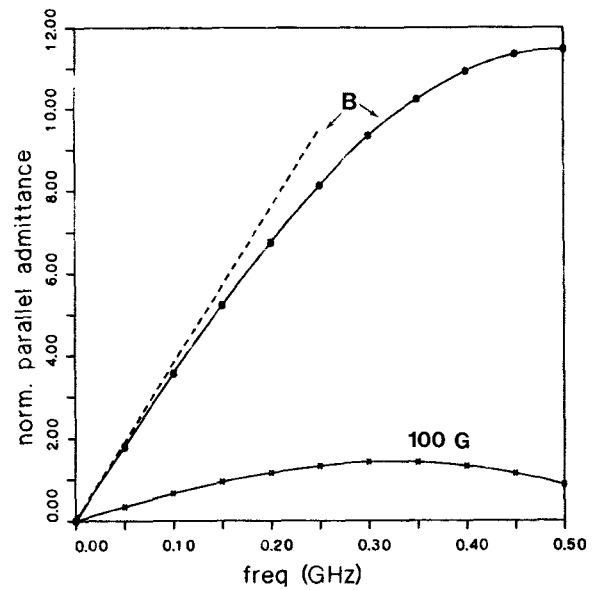
tively, the quasi-static values ωL_0 and ωC_0, obtained with (14) and (21).

VII. CONCLUDING REMARKS

The mixed potential integral equation has been found to be a very convenient tool for studying microstrip structures. Combined with a method of moments using subsectional basis, this technique can easily analyze conductors of irregular shape. Also, the MPIE remains valid at any frequency and can be used for studying higher order resonances as well as for characterizing microstrip discontinuities well below the first resonance. Thus, the techniques described in this paper are particularly useful for problems where the frequency is too high for assuming a quasi-static situation, but still too low for computing the fields as expansions over the resonant modes.

In this paper, we have also pointed out the connections existing between the MPIE and other models used for microstrip. In particular the well-known static and quasi-static integral equations are embedded in the MPIE, and this explains why the proposed algorithms are successful in providing first-order corrections to static capacitances and steady-state inductances.

Convergence studies have shown that cells of linear dimensions 0.05 λ already give good results. Under this condition, accurate theoretical values are obtained for resonant frequencies, quality factors, and input impedances of patch resonators. For discontinuities, the optimum cell size to obtain an accurate equivalent circuit is mainly related to the geometry of the upper conductor.

The MPIE includes surface waves and radiation. Multilayered substrates can be accommodated by suitable modifications of the Green's functions. Handling multiple conductors at different levels (stacked patches) is only a

matter of increasing the number of unknowns. Finally, there are no theoretical restrictions to the substrate thickness, though some of the excitation models discussed should be improved to maintain good accuracy in the thick substrate case.

The techniques of this paper can be applied to obtain the equivalent circuit of any microstrip discontinuity. Exciting the discontinuity with two lines of finite length, we get a combined geometry whose transmission or chain matrix T is obtained with the MPIE. Since the chain matrices T_0 of each line are known, the chain matrix of the discontinuity T_D satisfies the relationship $T = T_0 T_D T_0$ and can be easily obtained. Work is in progress and results will be reported in the near future.
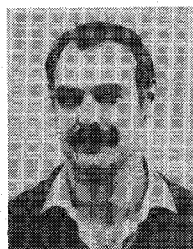
ACKNOWLEDGMENT

REFERENCES

[1] A. Farrar and A. T. Adams, "Matrix methods for microstrip three-dimensional problems," *IEEE Trans. Microwave Theory Tech.*, vol. MTT-20, pp. 497–504, 1972.

[2] P. Benedek and P. Silvester, "Capacitance of parallel rectangular plates separated by a dielectric sheet," *IEEE Trans. Microwave Theory Tech.*, vol. MTT-20, pp. 504–510, 1972.

[3] A. F. Thomson and A. Gopinath, "Calculation of microstrip discontinuities inductances," *IEEE Trans. Microwave Theory Tech.*, vol. MTT-23, pp. 648–655, 1975.

[4] P. Anders and F. Arndt, "Microstrip discontinuities capacitances and inductances for double steps, mitered bends with arbitrary angle and asymmetric right-angle bends," *IEEE Trans. Microwave Theory Tech.*, vol. MTT-28, pp. 1213–1217, 1980.

[5] T. S. Chu and T. Itoh, "Generalized scattering matrix method for analysis of cascaded and offset microstrip step discontinuities," *IEEE Trans. Microwave Theory Tech.*, vol. MTT-34, pp. 280–284, 1986.

[6] R. Chadha and K. C. Gupta, "Segmentation methods using impedance matrices for the analysis of planar microwave circuits," *IEEE Trans. Microwave Theory Tech.*, vol. MTT-29, pp. 71–74, 1981.

[7] R. Sorrentino, "Planar circuits waveguide models and segmentation method," *IEEE Trans. Microwave Theory Tech.*, vol. MTT-33, pp. 1057–1066, 1985.

[8] Y. Suzuki and T. Chiba, "Computer analysis method for arbitrarily shaped microstrip antenna with multiterminals," *IEEE Trans. Antennas Propagat.*, vol. AP-32, pp. 585–590, 1984.

[9] V. Palanisamy and R. Garg, "Analysis of arbitrarily shaped microstrip patch antennas using segmentation technique and cavity model," *IEEE Trans. Antennas Propagat.*, vol. AP-34, pp. 1208–1213, 1986.

[10] P. B. Katehi and N. G. Alexopoulos, "Frequency-dependent characteristics of microstrip discontinuities in millimeter-wave integrated circuits," *IEEE Trans. Microwave Theory Tech.*, vol. MTT-33, pp. 1029–1035, 1985.

[11] R. W. Jackson and D. M. Pozar, "Full-wave analysis of microstrip open-end discontinuities," *IEEE Trans. Microwave Theory Tech.*, vol. MTT-33, pp. 1036–1042, 1985.

[12] A. W. Glisson and D. R. Wilton, "Simple and efficient numerical methods for problems of electromagnetic radiation and scattering from surfaces," *IEEE Trans. Antennas Propagat.*, vol. AP-29, pp. 593–603, 1980.

[13] R. F. Harrington, *Field Computations by Moment Methods.* New York: Macmillan, 1968.

[14] J. R. Mosig and T. K. Sarkar, "Comparison of quasi-static and exact electromagnetic fields from a horizontal electric dipole above a lossy dielectric backed by an imperfect ground," *IEEE Trans. Microwave Theory Tech.*, vol. MTT-34, pp. 379–387, 1986.

[15] J. R. Mosig and F. E. Gardiol, "Analytical and numerical techniques in the Green's function treatment of microstrip antennas and scatterers," *Proc. Inst. Elec. Eng.*, pt. H, vol. 130, pp. 175–182, 1983.

[16] K. A. Michalski, "On the scalar potential of a point charge associated with a time-harmonic dipole in a layered medium," to be published in *IEEE Trans. Antennas Propagat.*

[17] J. R. Wait, *Electromagnetic Waves in Stratified Media.* Oxford: Pergamon Press, 1962.

[18] N. G. Alexopoulos and D. R. Jackson, "Fundamental superstrate (cover) effects on printed circuit antennas," *IEEE Trans. Antennas Propagat.*, vol. AP-32, pp. 807–816, 1984.

[19] P. Silvester and P. Benedek, "Electrostatics of the microstrip: Revisited," *IEEE Trans. Microwave Theory Tech.*, vol. MTT-20, pp. 756–758, 1972.

[20] P. D. Patel, "Calculation of capacitance coefficients for a system of irregular finite conductors on a dielectric sheet," *IEEE Trans. Microwave Theory Tech.*, vol. MTT-19, pp. 862–869, 1971.

[21] R. Crampagne, M. Ahmadpanah, and J. L. Guiraud, "A simple method for determining the Green's function for a large class of MIC lines having multilayered dielectric structures," *IEEE Trans. Microwave Theory Tech.*, vol. MTT-26, pp. 82–87, 1978.

[22] S. M. Rao, D. R. Wilton, and A. W. Glisson, "Electromagnetic scattering by surfaces of arbitrary shape," *IEEE Trans. Antennas Propagat.*, vol. AP-30, pp. 409–418, 1982.

[23] J. R. Mosig and F. E. Gardiol, "General integral equation formulation for microstrip antennas and scatterers," *Proc. Inst. Elec. Eng.*, pt. H, vol. 132, pp. 424–432, 1985.

[24] D. R. Wilton and A. W. Glisson, "On improving the stability of electric field integral equation at low frequency," presented at IEEE AP-S Int. Symp., Los Angeles, CA, June 1981.

[25] J. R. Mosig and F. E. Gardiol, "A dynamical radiation model for microstrip structures," in *Advances in Electronics and Electron Physics*, vol. 59. New York: Academic Press, 1982, pp. 139–237.

✳

Juan R. Mosig (S'76–M'87) was born in Cadiz, Spain, on December 18, 1951. He received the Electrical Engineer degree in 1973 from the Universidad Politecnica de Madrid. In 1975 he joined the Laboratory of Electromagnetics and Acoustics at the École Polytechnique Fédérale de Lausanne, Switzerland, from which he obtained the Ph.D. degree in 1983.

In 1984 he was a Visiting Research Associate at the Rochester Institute of Technology, NY. He is currently a Research Engineer at École Polytechnique Fédérale. His research interests include electromagnetic theory, numerical methods, and microstrip antennas.